Structure of ^{23}Al from a multi-channel algebraic scattering model based on mirror symmetry

P. R. Fraser[1,*], A. S. Kadyrov[1], K. Massen-Hane[1], K. Amos[2,3], L. Canton[4], S. Karataglidis[2,3], D. van der Knijff[2], and I. Bray[1]

E-mail: * paul.fraser@curtin.edu.au
[1] Department of Physics, Astronomy and Medical Radiation Sciences, Curtin University, GPO Box U1987, Perth 6845, Australia
[2] School of Physics, University of Melbourne, Victoria 3010, Australia
[3] Department of Physics, University of Johannesburg, P.O. Box 524 Auckland Park, 2006, South Africa
[4] Istituto Nazionale di Fisica Nucleare, Sezione di Padova, Padova I-35131, Italia

Abstract. The proton-rich nucleus ^{23}Al has a ground state just 123 keV below the proton drip-line, and as a result comparatively little is known experimentally about its properties, as with many such nuclei. Theoretical investigations have tended to model exclusively the ground and first one to three excited states known. In this paper, we theoretically model most of the known spectrum, and predict what states may as yet be unobserved. We use the multichannel algebraic scattering (MCAS) method to describe states as resonances of a valence proton coupled to a ^{22}Mg rotor core. Six states with low-excitation energies and defined J^π are matched, and we make the first prediction of the properties of four others and propound the possible existence of several more.

PACS numbers: 21.10.Ft, 21.60.Ev, 25.40.-h

Submitted to: *J. Phys. G: Nucl. Phys.*

1. Introduction

The proton-rich nucleus ^{23}Al was first discovered in 1969 [1], but having only one bound state, 123 keV below the one-proton emission threshold, comparatively little is known about its properties. As a result, much experimental effort has been spent on it in recent years [2, 3, 4, 5, 6, 7, 8, 9, 10], filling in details of the low-energy resonant spectrum. Several positive-parity states have been measured, some of which with details tentatively known. No negative parity states have been observed, though several should exist at low energies. Theoretical investigation goes back many years, with an early example being Sherr's examination of the Coulomb displacement energy of the mirror pair ^{23}Ne and ^{23}Al. These he compared with those predicted by a shell model, as a part of a broad survey [11]. A more recent shell model investigation was undertaken using the OXBASH shell-model code [12] and the USD family of interactions [13]. Theoretical treatment of this pair as nucleon and mass-22 systems has been undertaken in the context of asymptotic normalisation coefficients (ANCs) in capture reactions [14, 15] (and references therein).

Most of those theoretical studies concentrated upon the Gamow window region and so tend to focus only upon the ground and one or few low excitation resonance states. There are more resonance states in the known spectrum and we seek a description of this currently known spectrum.

We use the multi-channel algebraic scattering (MCAS) method to predict spectral properties of ^{23}Al to ∼4 MeV excitation, and to obtain elastic scattering cross sections. The method solves the coupled-channel problem of a nucleon coupled to a number of states in a 'core' nucleus. Lippmann-Schwinger equations for the coupled-channel problem are solved in momentum space starting with a set of coupled-channel interactions defined in coordinate space. They are specified using a collective model prescription. Those coupled-channel interactions are expanded using a set of Sturmian functions, and the coupled-channel Green's function is determined via an iterative process [16].

The coupled-channels scattering potentials of the system are formed with a target described by a Tamura collective model of rotor character [17], coupled to the projectile nucleus. The basic potential used for is

$$V_{c'c}(r) = f(r)\Big\{ V_0\delta_{c'c} + V_{ll}[\ell\cdot\ell]_{c'c} + V_{ss}[\mathbf{s}\cdot\mathbf{I}]_{c'c} \Big\} + g(r)V_{ls}[\ell\cdot\mathbf{s}]_{c'c} \ , \quad (1)$$

where c and c' denote channels, V_0 is the central potential strength, $V_{\ell\ell}$ is the orbital angular momentum dependent potential strength, $V_{\ell s}$ is the spin-orbit potential strength, and V_{ss} is the spin-spin potential strength, with all parameters in MeV. The channels (c) denote the underlying set of unique quantum numbers for each value of the total spin-parity of the compound system (J^π). The potentials are taken to have a Woods-Saxon form,

$$f(r) = \left[1+\exp\left(\frac{r-R_0}{a_0}\right)\right]^{-1} \quad ; \quad g(r) = \frac{1}{r}\frac{df(r)}{dr} \quad (2)$$

and matrix elements are shown in detail in Ref. [16]. This potential is then expanded to second order in terms of deformation of the nucleus. Full details of the expansion and the final form are provided in the Appendix of Ref. [18].

To account for the effects of Pauli blocked orbitals, orthogonalizing pseudo-potentials (OPP) are utilised. The OPP method was developed from the Orthogonality Condition Model of Saito [19]. The original potential, $V_{c\,c'}(\boldsymbol{r})$, is modified by adding OPP to define

$$\mathcal{V}_{cc'}(\boldsymbol{r},\boldsymbol{r'}) = V_{cc'}(\boldsymbol{r})\,\delta(r-r') + \lambda_c\,A_c(\boldsymbol{r})A_{c'}(\boldsymbol{r'})\delta_{cc'}\ , \quad (3)$$

where $A_c(\boldsymbol{r})$ is the single-nucleon radial wave function of an occupied orbital. For OPP to block the Pauli-forbidden orbitals, the blocking parameter, λ_c is set ostensibly to infinity, but 10^6 MeV suffices in practice. Though not used here, OPP blocking energies can be set at values between zero and infinity, for cases of 'hindrance' from partially filled orbitals [20]. Full details are presented in Ref. [21].

Consequently, the MCAS approach is particularly suitable for studying properties of the first few MeV of the spectra of systems such as ^{23}Al, which may be considered in that regime as a nucleon plus (core) nucleus clusters. Further, as the method readily gives scattering amplitudes, it enables prediction of cross sections for low-energy nucleon scattering from those 'core' nuclei in which resonance states of the compound can have effect.

To calculate a spectrum for ^{23}Al, we first study the mirror system, ^{23}Ne, as a n+^{22}Ne cluster so defining the nuclear part of the p+^{22}Mg Hamiltonian. Results for the spectrum of ^{23}Ne are given in Section 2 for completeness. They differ slightly from those published recently [22], as in that publication the model parameters were tuned to the case where coupling to one less target state was considered.

The nuclear interaction so defined is then used for the p+^{22}Mg system. In Section 3 a discussion is presented regarding the form of the Coulomb interactions added (with an alternative form discussed in Appendix A), and in Section 4 we give a prediction of the spectrum of ^{23}Al. Cross sections for elastic scattering of protons from ^{22}Mg from $E_{lab} = 0$ to 3 MeV are also shown and discussed therein. (Data at energies higher than the potential is designed for

are examined in Appendix B.) In Section 5, we present results obtained when the number of target nuclear states, used in the coupled-channel calculations, is reduced to that previously deemed [9] to contribute to the ground state of 23 Al. Finally, in Section 6 we draw our conclusions.

2. The nuclear interaction from the n+^{22}Ne system

In a recent paper [18], a good match was obtained between experiment and MCAS calculation for the excitation energies of the nine lowest eigenstates of ^{23}Ne, treated as the n+^{22}Ne system. These are all deeply bound with regard to the neutron emission threshold. Those states span an energy range of ∼3.5 MeV. At energies higher than this, processes other than coupling of a single particle to a collective target with two rotor-like bands come into effect.

The coupled channels for the mirror n+^{22}Ne study were formed using a rotational model description of the lowest five states of ^{22}Ne. The three lowest energy states were taken to be states of the principle rotor band; the $0^+_{g.s.}$, the 2^+_1 state (1.274 MeV in ^{22}Ne and 1.247 MeV in ^{22}Mg), and the 4^+_1 state (3.357 MeV in ^{22}Ne and 3.308 MeV in ^{22}Mg). Next we add the 4^+_2 state at 5.523 MeV excitation in ^{22}Ne (5.293 MeV in ^{22}Mg). We include this state since, recently, the one-proton knock-out reaction from the ground state of ^{23}Al was studied experimentally by Banu *et al.* [9], with γ-rays from the resultant excited ^{22}Mg indicating which states of that nucleus combine with a proton to populate the ^{23}Al ground state. Three γ-transitions were observed, $4^+_2 \rightarrow 4^+_1$, $4^+_1 \rightarrow 2^+_1$, and $2^+_1 \rightarrow 0^+_1$. However, while this experiment suggests that only these four target states are relevant to defining the ^{23}Al ground state, we seek to define more states than the ground state. Thus, the fourth known state of the spectrum, the 2^+_2 state (4.456 MeV in ^{22}Ne and 4.402 MeV in ^{22}Mg) was included. This state, like the 2^+_1 state, $E2$-decays to the ground [23]. In ^{22}Mg, the 4^+_2 also γ-decays to the $0^+_{g.s.}$ [23], 2^+_1 (characterised as $M1$ [23] + $E2$ [24]) and 4^+_1 [23] states. Thus, we expect it to play a role in channel coupling, even if not significantly with regard to the ground state of ^{23}Al. This is discussed in Section 5.

All of the above experimentally-known γ-transitions are summarised in Fig. 1. We note that in the case of ^{22}Mg, most possible decays between these five states have been observed experimentally, with four exceptions: there have been no observed $4^+_2 \rightarrow 2^+_2$, $4^+_2 \rightarrow 2^+_1$, $4^+_2 \rightarrow 0^+_1$, or $4^+_1 \rightarrow 0^+_1$ transitions. In our calculations we still assume all couplings, however.

The 2^+_2 and 4^+_2 states are not members of the main rotor band, but they can still be considered using the rotational model. Assuming a shape co-existence, these appear part of the second $K = 0$ β-band, though no 0^+_2 band head has been clearly observed. Alternatively, they may be the first and third states of a $K = 2$ γ-band, in which case all states should possess the same deformation, though no 3^+_2 state, the second state in such a band, has been clearly observed [25]. There is an uncertainly-assigned state in ^{22}Mg, denoted $(0^+, 1, 2, 3, 4^+)$, at 5 MeV that could be either [24]. Here, we effectively treat these states as part of a secondary $K = 0$ rotor band.

We denote the quadrupole coupling deformation of the primary and secondary rotor band as β_2 and $\overline{\beta_2}$, respectively. Assuming shape co-existence, we determine the ratio of these two deformations by considering the mean lifetime of a state that γ-decays to the ground state, which is a function of the transition probabilities, and for $E2$ multipolarity this is:

$$\frac{1}{\tau} = 1.23 \times 10^9 \; E_\gamma^5 \; B(E2)\,, \qquad (4)$$

with τ in s, E_γ in MeV, and $B(E2)$ in e^2 fm^4. In ^{22}Ne, the $E2$ transitions of the 2^+ states at 1.275 and 4.456 MeV have half lives of 3.63(5) ps and 37(6) fs respectively [24]. Thus, from Eq. (4) we obtain $B(E2)\big|_{1.275} = 46.06$ and $B(E2)\big|_{4.456} = 8.67$ e^2 fm^4. The ratio of these values is 0.188, and given that, without considering band quantum numbers and going only to the first order, as $B(E2)$ values of a collective model with rotational character are proportional to β_2^2, $\overline{\beta_2} = 0.43\,\beta_2$. As the simplest possible formalism, we assume that couplings involving the 4^+_2 have the same $\overline{\beta_2}$.

Table 1 contains the parameters that define the nuclear potential used in calculation of both n+^{22}Ne and p+^{22}Mg. The positive-parity central well depth, V_0, differs from the value of -51.3 MeV used in Ref. [18], to bring the ^{23}Ne ground state energy, relative to the neutron emission threshold, in line with experiment to three decimal points. (In Ref. [18], the parameters were selected without consideration of the 4^+_2 state. The adjustment here is to address that.) β_4 indicates a small hexadecapole deformation, and R_0 and a_0 are radius and diffusivity of Eq. (2). The MCAS spectrum of ^{23}Ne found using the parameter set of Table 1 is compared to experiment in Fig. 2. This calculation results in a match, within 0.5 MeV, for the nine lowest-energy states known for which spin-parities are well assigned or postulated. This makes a good result for a range of up to 3.5 MeV.

There are three higher-spin states in the MCAS spectrum that have no currently known partner: a $\frac{9}{2}^+$ state at -5.061 MeV relative to the neutron emission threshold, a $\frac{13}{2}^-$ state at -3.565 MeV, and an $\frac{11}{2}^-$ state at -1.764 MeV. If a $\frac{9}{2}^+$ state existed at such

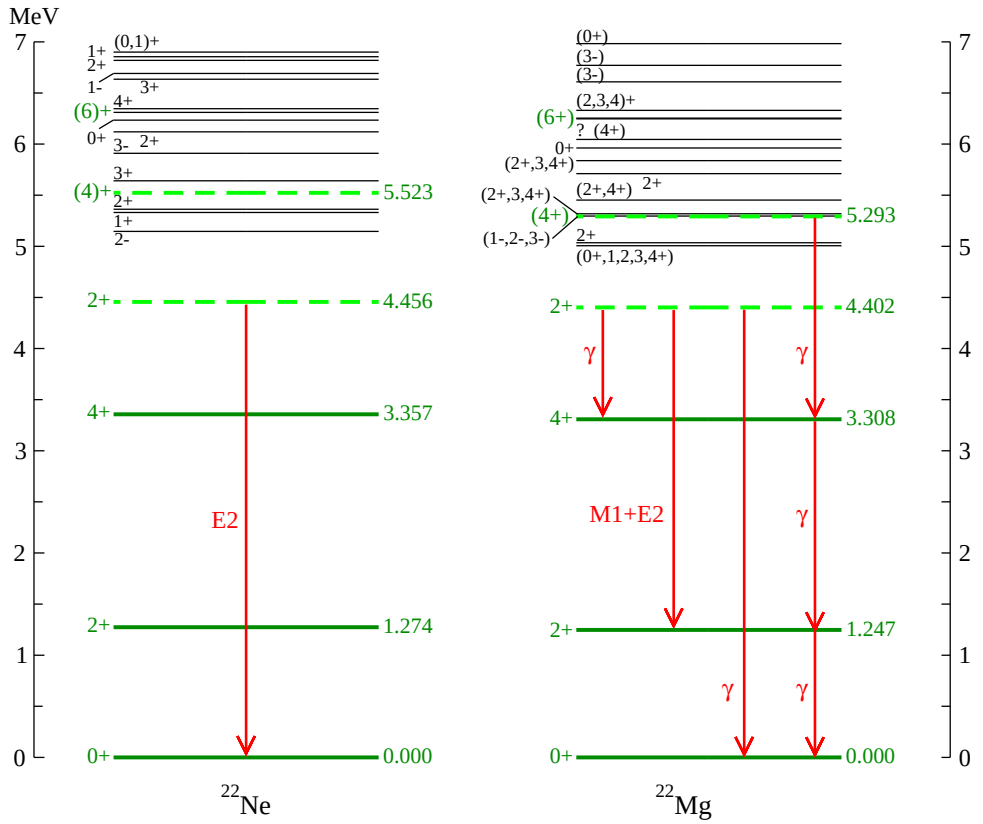

Figure 1. The low-energy experimental spectra of ^{22}Ne and ^{22}Mg. Solid, thick lines represent states of the main rotor band, and thick, dashed lines are states known to couple to them by γ-emission. Observed couplings between states in and out of the main rotor band shown by arrows. Data are from Ref. [9, 24, 23].

Table 1. Parameter values defining the n+^{22}Ne interaction. $\lambda^{(OPP)}$ are blocking strengths of occupied shells, in MeV, with the same values used for all target states considered.

	Odd parity	Even parity
V_0 (MeV) Fig. 2 & 4	-65.200	-50.894
V_0 (MeV) Fig. 5	-64.620	-50.372
V_0 (MeV) Fig. 8	-64.825	-50.650
V_0 (MeV) Fig. B1	—	-49.650
V_{ll} (MeV)	-1.01	-0.30
V_{ls} (MeV)	7.00	7.00
V_{ss} (MeV)	-0.20	-1.45

R_0	a_0	β_2	$\overline{\beta_2}$	β_4
3.1 fm	0.75 fm	0.22	0.1034	-0.08

	$1s_{1/2}$	$1p_{3/2}$	$1p_{1/2}$	$1d_{5/2}$
$\lambda^{(OPP)}$	10^6	10^6	10^6	0.0

$\overline{\beta_2}$ for linking 2_2^+ and 4_2^+ to each other and other states; 43% of 0.22.

low energy, it would likely have been observed in experiment by population of $E1$ Γ-emission from the $\frac{7}{2}^-_1$ state predicted in this work. This $\frac{7}{2}^-_1$ state is likely to exist near this energy, given the observation of such a state in ^{23}Ne. In this calculation, the state in question arises from coupling of the ^{22}Mg 2^+ and 4^+ states with protons of $\ell \leq 11$, as appropriate. To determine what partial probabilities the various coupled-channel components contribute requires calculation of co-ordinate space wavefunctions, which is future work. As it is known from Ref. [9] that three of these states of ^{22}Mg are involved in the ground state of ^{23}Al, it is reasonable to expect that a low-energy $\frac{9}{2}^+$ state exists, but with a higher energy than that calculated. This likely indicates the need for a more-refined scattering potential.

While there is room for further elaboration of this potential, including better accounting for the difference in inter- and intra-band coupling strengths, and consideration of Pauli hindrance [21], this potential suffices for making predictions of the cross section of the mirror system, p+^{22}Mg, and the spectrum of the compound system, ^{23}Al. For this, a suitable charge distribution of ^{22}Mg is necessary.

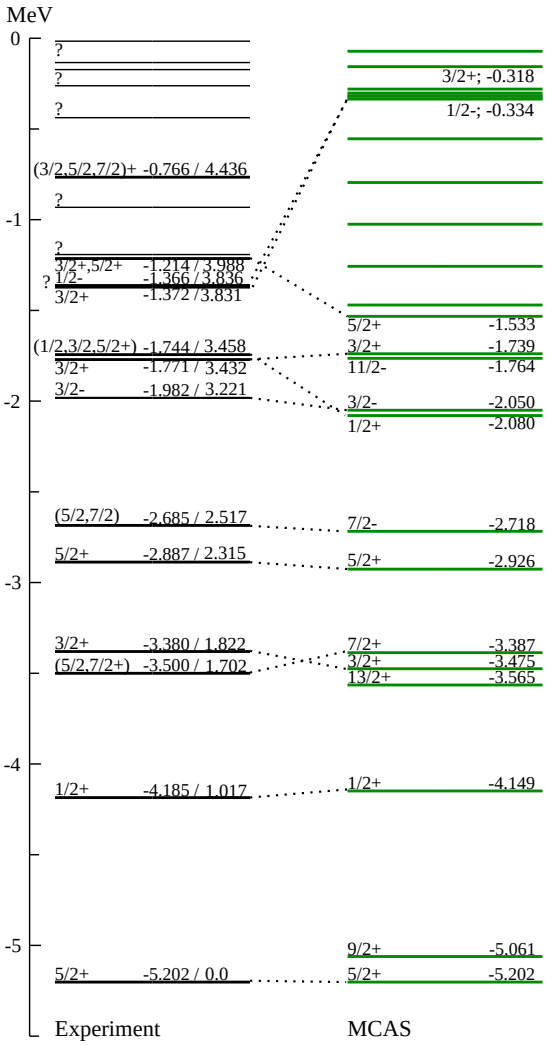

Figure 2. The experimental ^{23}Ne spectrum [26] and that calculated from MCAS evaluation of the n+^{22}Ne, with target state set 0^+_1, 2^+_1, 4^+_1, $\overline{2^+_2}$ and $\overline{(4)^+_2}$. The bar denotes the use of reduced coupling for channels involving this state. In the experimental spectrum, energies before the slash are relative to the one-proton emission threshold, and energies after are relative to the ground state.

3. The Coulomb interaction for the p+^{22}Mg system

Experimental measurement of the root-mean-square (rms) charge radius of the stable and long-lived nuclei was mostly completed in the 1980s, and parameterisations of charge distribution functions for these are available [27]. These have recently been used in MCAS studies [22, 28]. However, such experimental guidance is not yet available for radioactive ion beam (RIB) nuclei, though the SCRIT experiment at the RIKEN RIB Factory [29, 30] has begun taking data.

In the interim, charge-distribution information from other theories may be used in generating Coulomb potentials for calculations of proton-nucleus cluster structure and proton scattering with these nuclei. One such theory, the relativistic mean-field (RMF) model [31], was used recently by Wang and Ren [32, 33] to calculate charge distributions for light proton-rich nuclei, the properties of which they later compared with standard parameterised functions of charge distribution [34]. In particular, they found an RMF charge distribution for ^{22}Mg with an rms charge radius, $R^{(c)}_{rms}$, of 3.088 fm, and this is used here to derive the Coulomb potential for p+^{22}Mg scattering. This charge distribution and the Coulomb potential are shown in panel (a) and (b) of Fig. 3, respectively. Additionally, panel (b) shows the Coulomb potential that results from assuming a point-like ^{22}Mg target, i.e., $V_{Coul} = 12\ e^2\ /\ r$. This indicates that the asymptotic behaviour of the potential derived from the charge distribution is correct.

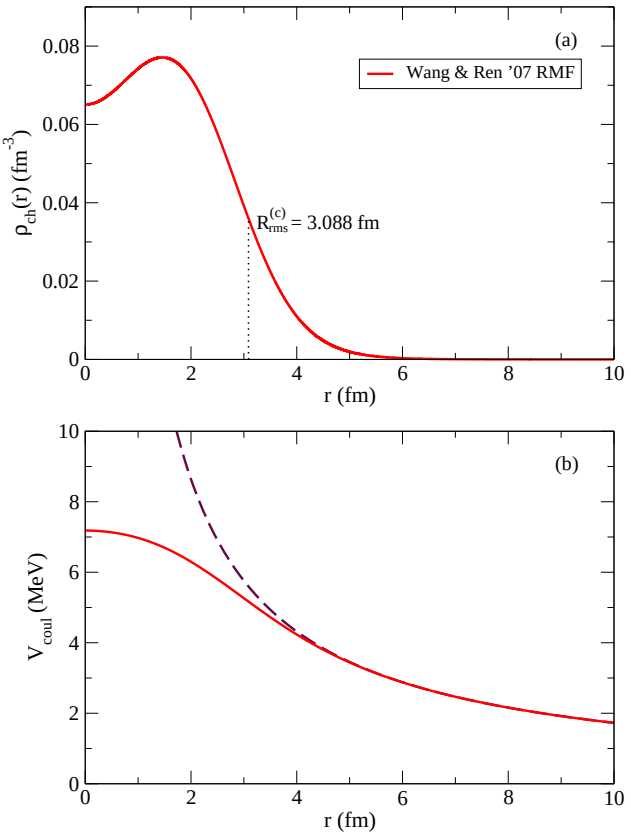

Figure 3. (a) RMF model theoretical charge distribution for ^{22}Mg from Ref. [33]. (b) Resultant Coulomb potential (solid line) and potential assuming point-like target (dashed line).

In Appendix A, the use of Coulomb potentials generated from three-parameter Fermi (3pF) charge distributions is investigated, and compared to the results from the RMF charge distribution.

4. Observables of the p+^{22}Mg system

The compiled spectrum of ^{23}Al consists of eight states [26], of which only the ground state is bound, with the one-proton separation energy being 123 keV. The ground state and first known excited state at 0.55 MeV have angular momentum and positive parity firmly assigned, as well as measured half-lives. Five more states have firmly assigned positive parity and tentative angular momentum. Only the excitation energy is known of the remaining state. Since that compilation, He *et al.* [4] found four resonances in ^{1}H(^{22}Mg, p)^{22}Mg scattering with E_x = 3.00, 3.14, 3.26 and 3.95 MeV. By R-matrix analysis, they argue that the first and last of these may have spin-parity $\frac{3}{2}^+$ and $\frac{7}{2}^+$, respectively. The state at 3.00 MeV is a likely partner to the $\frac{3}{2}^+$ state in ^{23}Ne at 3.432 MeV above the ground state. The states at 3.14 and 3.26 MeV were both tentatively assigned as $(\frac{7}{2}^+, \frac{5}{2}^+)$. Gade *et al.* [5] measured a state 1.616 MeV above the ground state which they argued to have spin-parity $\frac{7}{2}^+$, of which a probable partner, currently assigned $\left(\frac{5}{2}, \frac{7}{2}^+\right)$, is known in ^{23}Ne 1.701 MeV above the ground state. Certainly, though, the low-energy spectrum will be much richer than that so far observed.

4.1. Charge symmetry

Fig. 4 shows the MCAS spectrum of ^{23}Al that results from using the parameter set of Table 1, with the addition of the Coulomb potential derived from the charge distribution of Ref. [33]. This is compared to the few observed states of ^{23}Al. Each experimentally observed state has a theoretical partner nearby, though all are overbound. The ground state is overbound by ∼229 keV. A deviation of similar magnitude has been observed from studies of other mirror systems with MCAS calculations made using Coulomb interactions defined from charge distributions with the known rms charge radii [22]. In those cases the deviation could possibly be ascribed to nuclear effects (possibly charge symmetry breaking). See Appendix A for a study of the impact of the choice of Coulomb potential used.

4.2. Adjusted charge symmetry

As the p+^{22}Mg central potential depth, V_0, is much greater than the other components of the nuclear potential, slight adjustments can be used to alter the binding of all calculated compound states without altering the spacing between them. Using the RMF-derived charge distribution from Ref. [33], a value of -50.372 MeV for the central well depth for positive parity states, V_0^+, reduces the ground state binding by the 229 keV necessary to obtain a match with data.

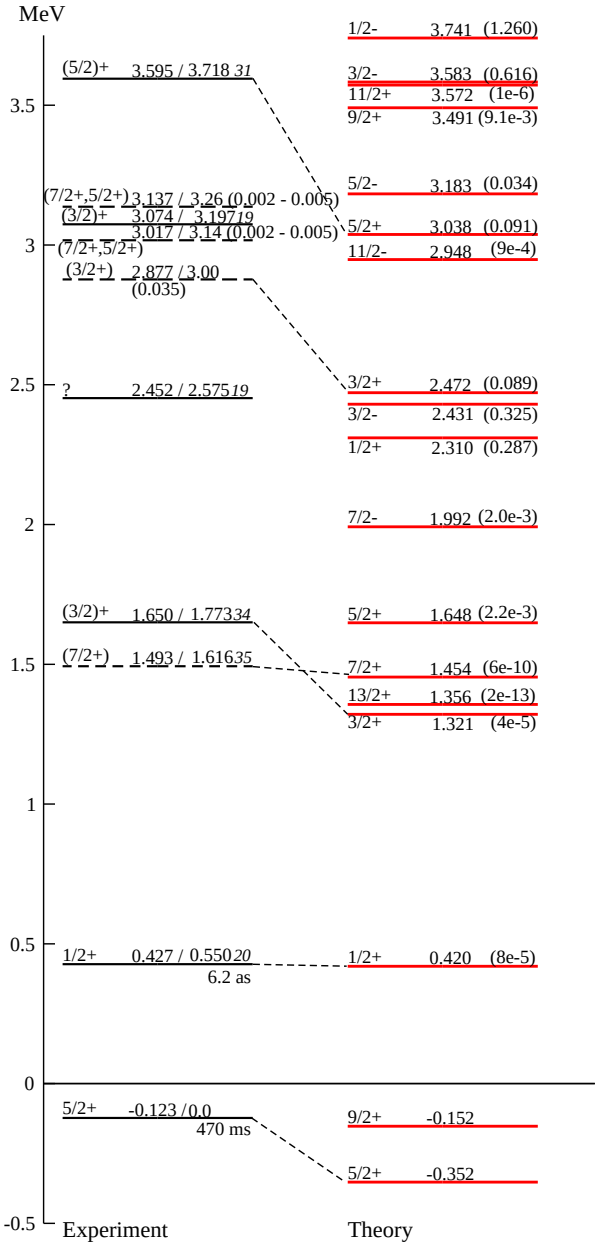

Figure 4. (Color online.) The known experimental ^{23}Al spectrum (solid lines [26], long dashed lines [4], short dashed lines [5]) and that calculated from MCAS evaluation of the p+^{22}Mg, with target state set 0_1^+, 2_1^+, 4_1^+, $\overline{2_2^+}$ and $\overline{(4)_2^+}$, with charge distribution from Ref. [33]. Parameters are as per Table 1, with $V_0^- = -65.200$ MeV and $V_0^+ = -50.894$ MeV. The bar denotes the use of reduced coupling for channels involving this state. In the experimental spectrum, energies before the slash are relative to the one-proton emission threshold, and energies after are relative to the ground state. Uncertainties are shown in italics. In the 'Theory' spectrum, unbracketed values are level energy relative to one-proton emission threshold. Bracketed values are full width at half maximum. All energies are in MeV.

For the same increase in energy of the first calculated negative parity state, with $J^\pi = \frac{7}{2}^-_1$, a value of -64.620 MeV is used for the negative parity states' central well depth, V_0^-. The resultant spectrum is shown in Fig. 5.

Thus, MCAS recreates the observed $\frac{5}{2}^+_1$, $\frac{1}{2}^+_1$, $\frac{3}{2}^+_1$, $\frac{7}{2}^+_1$, $\frac{3}{2}^+_2$ states, and the $\frac{5}{2}^+$ state observed at 3.595 MeV above the one-proton emission threshold, though the spins of all but the lowest two are uncertain. The model gives many more resonance states in the low excitation region and it remains to be seen if such have any empirical matches. The resonance widths found are solely for one-proton emission, which is not problematic as the energies considered are below the emission thresholds for α-particles (8.58 MeV above the ground state), deuterons (17.28 MeV), neutrons (19.48 MeV) and tritons (25.75 MeV). Γ-decay channels, while open, have negligible widths compared to particle emissions. This is illustrated, for example, for the $\frac{1}{2}^+_1$ state by Table IV of Ref. [3].

The model predicts a $\frac{5}{2}^+$ state (in Fig. 5 at 1.826 MeV) not observed thus-far, in addition to the ground state and putatively assigned $\left(\frac{5}{2}\right)^+$ state observed at 3.595 MeV above the one-proton emission threshold. It also predicts, relative to that threshold, a $\frac{7}{2}^-_1$ at 2.222 MeV, a $\frac{1}{2}^+_1$ at 2.486 MeV, and a $\frac{3}{2}^-_1$ state at 2.658 MeV. However, if the other known states in the region are a guide, it might be expected that those states exist ∼0.5 MeV higher than MCAS predicts. Furthermore, with this potential MCAS predicts several states around 3.5 MeV (relative to the one-proton emission threshold), and two high-spin states at lower energies. These may correspond to the partially defined states observed in this region. To obtain a better match to the three highest energy states observed experimentally, being two $\left(\frac{7}{2}\right)^+$ states at 3.95 MeV and 4.2 MeV, and a $\left(\frac{5}{2}\right)^+$ at 11.8 MeV, all relative to the ground state, requires improvement to the model specification of the channel coupling interactions and, possibly taking more states of ^{22}Mg into account.

In Table 2, the MCAS results are compared with experimental data and those of other calculations reported in the literature [5, 13, 26, 35]. The shell-model calculation of Ref. [13] concerned itself with only the four lowest-energy states known in ^{23}Al, $\frac{5}{2}^+_1$, $\frac{1}{2}^+_1$, $\frac{3}{2}^+_1$ and $\frac{7}{2}^+_1$, making no predictions. We tabulate their calculation which uses the USD*($V^{pn}_{T=1}$) interaction, as this provided them their best match to experimental data. (Note that in their Table IV they appear to have the labels of the $\frac{3}{2}^+_1$ and $\frac{7}{2}^+_1$ states reversed.) Ref. [14] calculated properties of the $\frac{1}{2}^+_1$ resonance, obtaining an excitation energy of 0.405 MeV, and a proton

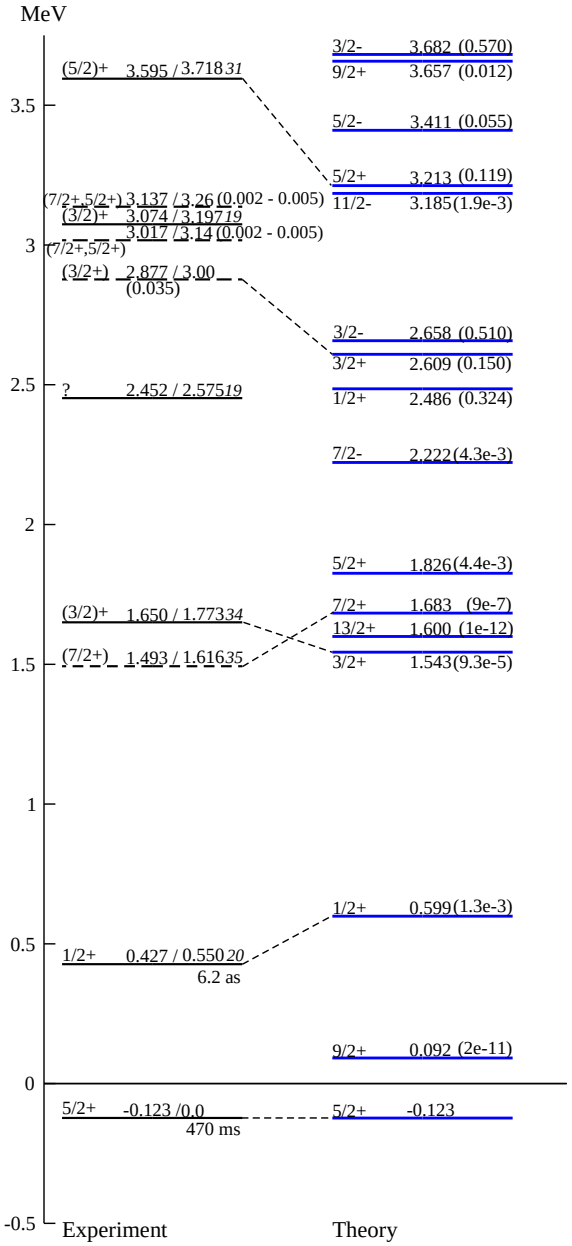

Figure 5. (Color online.) The known experimental ^{23}Al spectrum [4, 5, 26], and that calculated from MCAS evaluation of the p+^{22}Mg, relative to the one-proton emission threshold. The MCAS results are obtained with target state set 0^+_1, 2^+_1, 4^+_1, $\overline{2^+_2}$ and $\overline{(4)^+_2}$, with charge distribution from Ref. [33]. Parameters are as per Table 1, with $V_0^- = -64.620$ MeV and $V_0^+ = -50.372$ MeV. The bar denotes the use of reduced coupling for channels involving this state. In the experimental spectrum, energies before the slash are relative to the one-proton emission threshold, and energies after are relative to the ground state. Uncertainty in italics. In the 'Theory' spectrum, unbracketed values are energy levels relative to one-proton emission threshold. Brackets values are full widths at half maximum. All energies are in MeV.

width of 2.01×10^{-2} MeV and 9.19×10^{-2} MeV from a multichannel and a single-channel microscopic cluster model, respectively. Ref. [15] reports on calculations focused solely on the ground state and $\frac{1}{2}^+_1$ state of ^{23}Ne and ground state of ^{23}Al, obtaining agreement with experiment to three decimal places. Their interest, however, was with capture reactions and so they used a simple model which couples a valence nucleon to a rotor core [36], without some of the features of the MCAS model used herein, and with only the 0^+, 2^+ and 4^+ states of the core-nucleus' primary rotor band. Based on the results of Ref. [18] and Section 5 of this work, it may be interesting for them to repeat their investigation including also the 2^+_2 core state. Ref. [4] reported four new states between 3 and 4 MeV above the ground state, and provided tentative J^π designations based on measurement and on R-matrix fits, Table 2 quoting the those suggested by measurement. Finally, in Ref. [5] a theoretical estimate of the width of the $\frac{7}{2}^+_1$ state they measured was made using an USDB shell model calculation.

Widths for the three lowest-energy resonances known, both experimental and theoretical, are extremely small in all investigations. Regarding the $\frac{1}{2}^+_1$ state, the result of Ref. [14] is of the same order as the experimental result, where the MCAS result is larger. With MCAS, the excitation energy of this state is overestimated by 0.17 MeV. The microscopic cluster model [14] underestimated the energy of that state by about the same amount. This state is important in any study of resonant capture and, as such reactions are planned for future MCAS studies, more detailed analyses leading to more accurate properties for this state will be needed. However, as the goal in the present work is to predict the spectrum over several MeV, rather than focusing solely on the Gamow window, this discrepancy is not of prime concern here. The excitation energies of the first four observed states reported in Ref. [13] are closer to experiment than we have found here, and closer to experiment than the $\frac{1}{2}^+_1$ result in Ref. [14]. Ref. [13] presents no information for higher-energy states. The $(\frac{3}{2}^+)$ measured at 3.00 MeV in Ref. [4] is the only state of that work for which the MCAS calculation finds a match. The width of this state found by MCAS is five times that of the measurement of Ref. [4]. The other states of Ref. [4] are not recreated as these are in an energy regime that is higher than where this MCAS calculations is most accurate.

4.3. Elastic scattering cross sections

Fig. 6 shows several low-energy elastic scattering cross sections obtained using the charge distribution of Ref. [33] and the same nuclear parameter set as for the

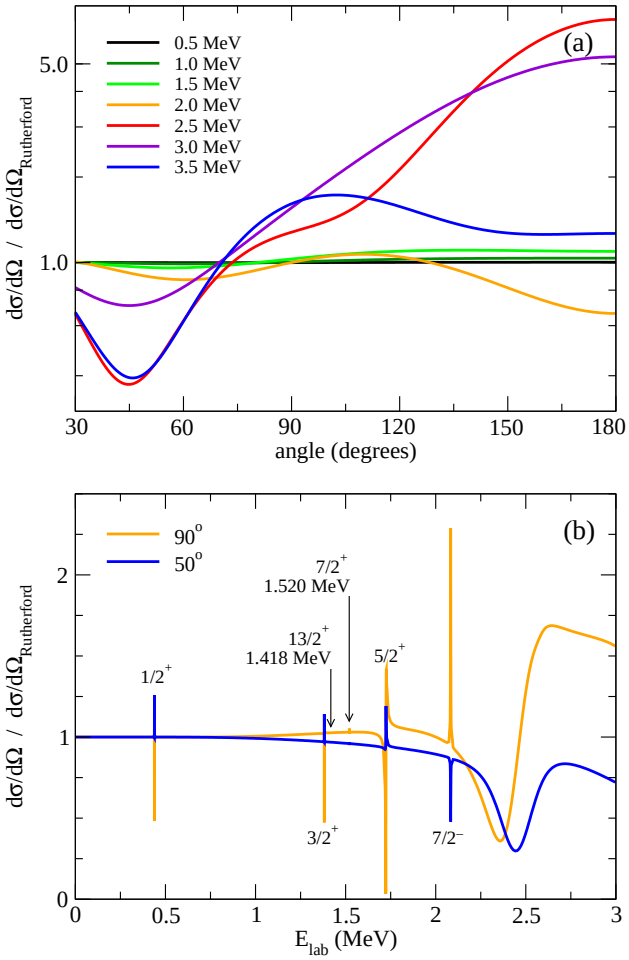

Figure 6. (Color online.) (a) p+^{22}Mg elastic scattering cross section at several fixed proton laboratory energies (b) p+^{22}Mg elastic scattering cross section at fixed angles 50^o and 90^o for proton energies from 0.0 to 3.0 MeV. All presented as ratio to Rutherford cross sections. Parameters are as per Table 1, with $V_0^- = -65.200$ MeV and $V_0^+ = -50.894$ MeV.

n+^{22}Ne investigation. Fig. 7 presents cross sections that result from the adjustment of V_0^+ and V_0^- detailed previously.

Comparing panels (a) in Figs. 6 and 7, the differential cross sections at 0.5, 1.0, 1.5 and 2.0 MeV, being in an energy region where only narrow compound states are calculated, change little with the adjustment of state excitation energies. The cross sections at 2.5, 3.0 and 3.5 MeV differ dramatically, as would be expected from the number of compound states with large widths calculated in this energy region and moved by the change in parameters.

Comparing panel (b) in each figure, the cross sections remain very similar until ∼2.25 MeV. Changing the V_0^+ parameter from -50.894 MeV to -50.372 MeV removes the good agreement the $\frac{1}{2}^+_1$ excitation energy had with experiment in Fig. 4, but

Table 2. Resonance energies, relative to ground state, and decay widths of states in ^{23}Al determined from experiment, MCAS, and calculations in the literature. E_x is the excitation energy, Γ_p is the one-proton emission width. All energies are in MeV. The OXBASH [13] result is their best match to data. The two Γ_p values from [14] are their single- and multi-channel results, respectively.

	Compiled data [26]		Exp.	Shell model [5]	Exp. [4]		MCAS Fig. 5		Microscopic cluster model [14]		OXBASH [13]
J^π	E_x	Γ_p	E_x	Γ_p	E_x	Γ_p	E_x	Γ_p	E_x	Γ_p	E_x
$\frac{5}{2}^+$	0.0	N/A					0.0	N/A			0.0
$\frac{1}{2}^+$	0.55	7.4×10^{-5}					0.722	1.30×10^{-3}	0.405	2.01×10^{-5}	0.57
										9.19×10^{-5}	
$(\frac{7}{2}^+)$			1.616	1.1×10^{-9}			1.806	8.70×10^{-7}			1.56
$(\frac{3}{2})^+$	1.773						1.666	9.32×10^{-5}			1.70
?	2.575						see below line				
$(\frac{3}{2}^+)$					3.00	0.032	2.732	0.1504			
$(\frac{7}{2}^+, \frac{5}{2}^+)$					3.14	2 - 5 keV					
$(\frac{3}{2})^+$	3.197										
$(\frac{7}{2}^+, \frac{5}{2}^+)$					3.26	2 - 5 keV					
$(\frac{5}{2})^+$	3.718						3.336	0.1192			
$(\frac{7}{2}^+)$					3.95	0.02					
$(\frac{7}{2})^+$	4.200						-	-			
$(\frac{5}{2})^+$	11.78						-	-			
$\frac{9}{2}^+$							0.215	2.2×10^{-11}			
$\frac{13}{2}^+$							1.723	1.3×10^{-12}			
$\frac{5}{2}^+$							1.949	4.42×10^{-3}			
$\frac{7}{2}^-$							2.345	4.32×10^{-3}			
$\frac{1}{2}^+$							2.609	0.325			
$\frac{3}{2}^-$							2.781	0.511			

in the cross sections the corresponding resonance is of extremely narrow width. This means that the non-resonant part of the cross section calculated in this energy regime in Fig. 7 might be a reasonable prediction. Importantly, the unobserved $\frac{9}{2}^+$ and $\frac{13}{2}^+$ states found in the spectral calculation do not appear in the calculated cross sections. Above ∼2.25 MeV, the larger-width $\frac{5}{2}^+$, $\frac{5}{2}^-$, $\frac{9}{2}^+$ and $\frac{3}{2}^-$ resonances dominate the cross section, and therefore their excitation energies relative to states that may or may not exist here influence the quality of the predicted cross sections at these energies. It remains to be seen what resonant states at 2.5 MeV and higher exist before the accuracy of the cross sections calculated in this energy region may be assessed.

5. The effect of the 2_2^+ target state

When investigating which states of ^{22}Mg couple with a valence proton to form the ^{23}Al ground state, Banu *et al.* [9] did not observe the 2_2^+ state playing a role. We repeat the calculation of Fig. 5 using only the target-state set 0_1^+, 2_1^+, 4_1^+, and $\overline{(4)_2^+}$, to see if it erroneously plays a role in the calculated ground state, and if it need be considered in other states of ^{23}Al. Again, V_0^+ was adjusted to match the ground state to experiment. Without experimental guidance, V_0^- was adjusted to match the first predicted negative parity state, $\frac{7}{2}^-$, to the same energy as in Fig. 5. This gave the values $V_0^- = -64.825$ MeV and $V_0^+ = -50.650$ MeV. The resulting spectrum is compared to experimental eigenenergies in Fig. 8. In Fig. 9, the resulting fixed-angle cross sections are compared to those of Fig. 7.

It is seen that the $\overline{(2)_2^+}$ target state makes a negligible contribution to the ground state, in agreement with the experimental observation of Banu *et al.*. It also makes a negligible contribution to all other states in the calculated spectrum, with the following exceptions: its absence brings the calculated counterpart of the $\frac{1}{2}^+$ resonance, observed at 0.427 MeV above the one-proton emission threshold, into slightly better agreement with experiment; the energy of the calculated $\frac{13}{2}^+$ resonance is slightly increased; and the magnitude of cross sections is slightly reduced at the higher end of the calculated energy range. Additionally, the calculated widths of the resonances from this calculation are somewhat smaller than those of Fig. 5.

As the coupling of this state to the valence proton contributes to the $\frac{1}{2}^+$ state just above the one-proton removal threshold, its inclusion may be of importance for studies focused on that state, for example Ref. [36].

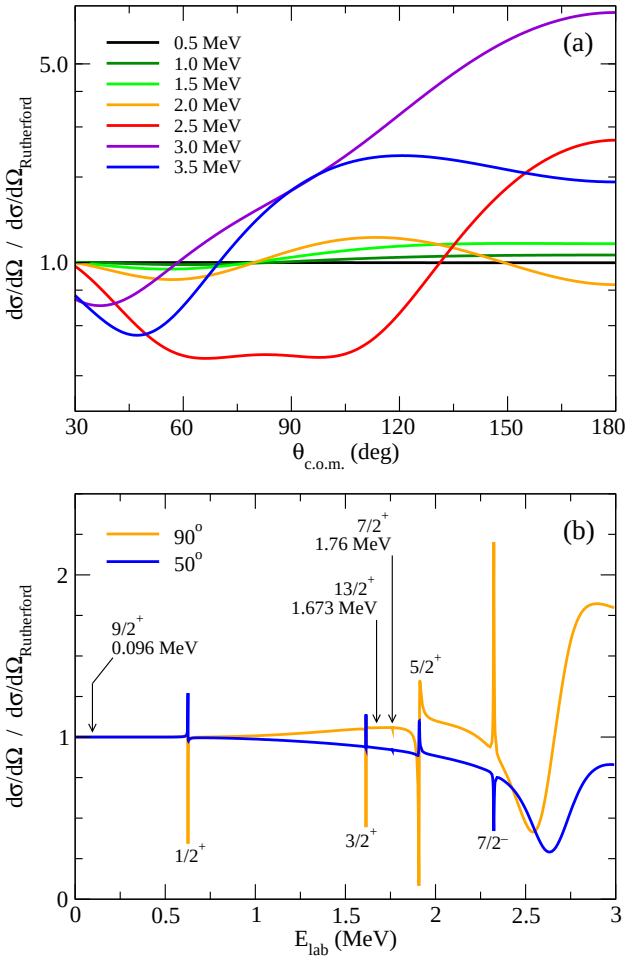

Figure 7. (Color online.) (a) p+^{22}Mg elastic scattering cross section at several fixed proton laboratory energies (b) p+^{22}Mg elastic scattering cross section at fixed angles 50^{o} and 90^{o} for proton from 0.0 to 3.0 MeV. All presented as ratio to Rutherford cross sections. Parameters are as per Table 1, with $V_0^- = -64.620$ MeV and $V_0^+ = -50.372$ MeV.

6. Conclusion

Relatively little is known experimentally about the low-energy spectrum of ^{23}Al, and we have endeavoured to perform the most comprehensive calculation of this spectrum to date, over several MeV. We have treated it as a clusterisation of a proton and ^{22}Mg, using a coupled-channel approach. Channels have been defined by five low excitation states in ^{22}Mg.

The nuclear interaction was determined using mirror symmetry and the related coupled-channel problem of the neutron+^{22}Ne cluster [18]. The five states of the core nucleus were deemed to be members of two rotation bands; the three lowest (0_1^+ g.s., 2_1^+, 4_1^+) belonging to a ground state rotation band. The 2_2^+ and 4_2^+ were assumed as members of a second band with coupling to the other three via a scaled strength. The deformation strengths defining these

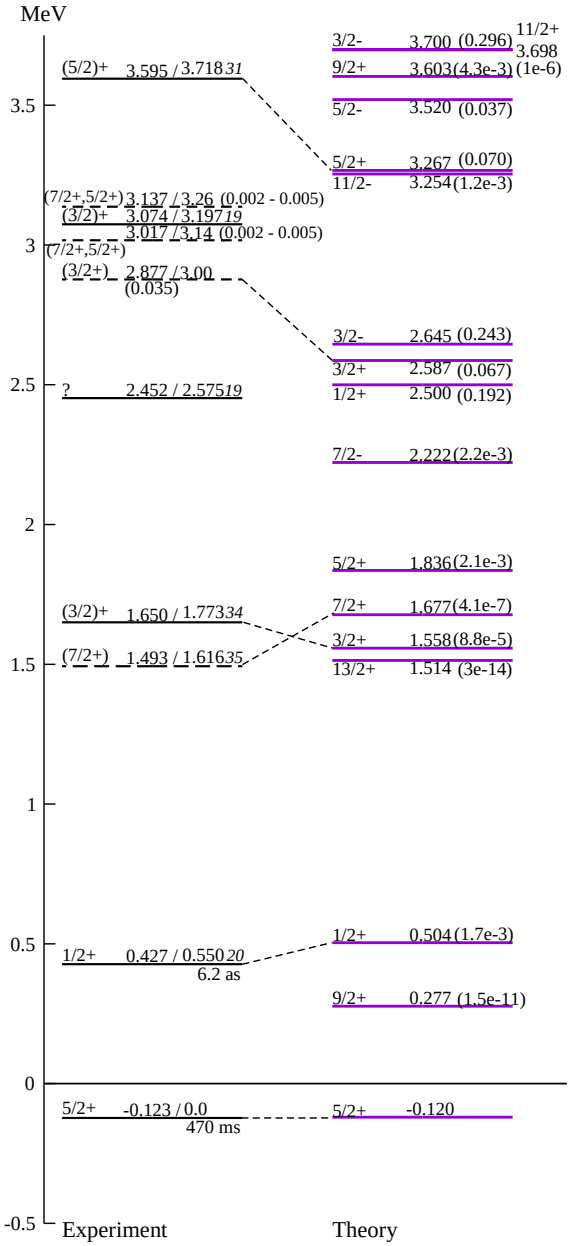

Figure 8. (Color online.) The known experimental ^{23}Al spectrum [4, 5, 26] and that calculated from MCAS evaluation of the p+^{22}Mg, relative to the one-proton emission threshold. The MCAS results are obtained with target state set 0_1^+, 2_1^+, 4_1^+, and $\overline{(4)_2^+}$, with charge distribution from Ref. [33]. Parameters are as per Table 1, with $V_0^- = -64.825$ and $V_0^+ = -50.650$. The bar denotes the use of reduced coupling for channels involving this state. In the experimental spectrum, energies before the slash are relative to the one-proton emission threshold, and energies after are relative to the ground state. Uncertainties are shown in italics. In the 'Theory' spectrum, unbracketed values are energy levels relative to one-proton emission threshold. Bracketed values are full widths at half maximum. All energies are in MeV.

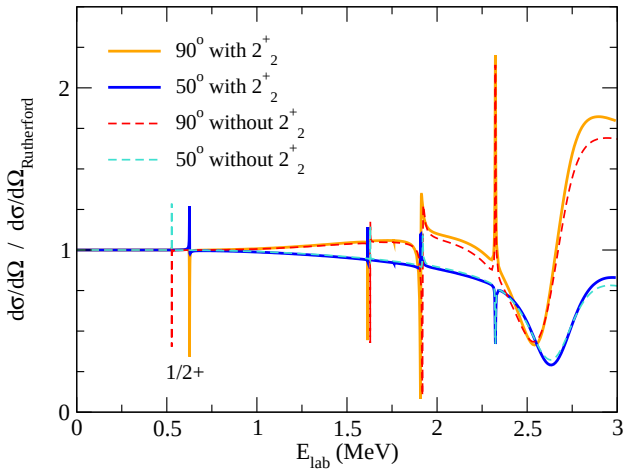

Figure 9. (Color online.) p+^{22}Mg elastic scattering cross section at fixed angles 50$^{\rm o}$ and 90$^{\rm o}$ for proton energies from 0.0 to 3.0 MeV, presented as ratio to Rutherford cross sections. Dashed lines are as per Table 1, with $V_0^- = -64.825$ MeV and $V_0^+ = -50.650$ MeV, with target state set 0^+_1, 2^+_1, 4^+_1, and $(4)^+_2$. Solid lines are as per Fig. 7.

couplings were linked to the known γ-decay properties (in ^{22}Ne). The 2^+_2 was found to contribute only to the $\frac{1}{2}^+$ state of ^{23}Al, supporting the findings of Banu *et al.* that it is not involved in the ground state. Coulomb interactions associated with a theoretical model of the charge distribution of ^{22}Mg [33] were used. The coupled-channel problems were solved using the MCAS procedure in which the Pauli principle effects were accommodated.

Where previous theoretical calculations have restricted themselves to just the ground state [15], the ground state and first known resonant state [14], or the four lowest energy states known [13], in this investigation, many ^{23}Al eigenstates in the first ∼3.5 MeV of the spectrum have been calculated, and low-energy elastic scattering cross sections have been presented at several energies and two fixed angles. After accounting for a small overbinding which may be due to charge symmetry breaking of the nuclear forces, a theoretical partner was found within ∼0.6 MeV for each state of the compound system with experimentally assigned J^π. Below ∼2.25 MeV, where placement of excitation energies is good, calculated proton-emission widths are very small, as are the one known experimentally and the other theoretical results available [5, 14]. Being very small, these do not have much influence on the scattering background, giving some confidence that the presented cross section calculations are reasonable predictions. Such was the case in past uses of MCAS for nucleons on ^{12}C [21, 37] and ^{14}O [20].

Obtaining the known spectrum of ^{23}Al through the threshold region as well as elastic scattering cross sections (protons from ^{22}Mg) is necessary for planned future evaluations of the capture process using MCAS [38], so that both the scattering and capture states can be defined by a single Hamiltonian. The capture of protons by ^{22}Mg has pertinence in specific nucleosynthesis problems. We intend, as future work, to build MCAS to evaluate capture cross sections and, for the case of proton capture by ^{22}Mg, an interaction then will be needed that gives better energy values for the ground and first excited states in ^{23}Al.

Acknowledgments

The authors gratefully acknowledge Z. Wang and Z. Ren for providing numerical results from their published nuclear charge distributions, and J. J. He and collaborators for providing their published p+^{22}Mg cross section data. This work was supported by the Australian Research Council. ASK acknowledges a partial support from the U.S. National Science Foundation under Award No. PHY-1415656. LC acknowledges funds from the Dipartimento di Fisica e Astronomia dell'Università di Padova. SK acknowledges support from the National Research Foundation of South Africa.

Appendix A. 3pF charge distributions

It is instructive to investigate also a simple parameterised functional form for the charge distribution of ^{22}Mg. We examine several cases of the three-parameter Fermi distribution [39], as this form recreates the central 'dip' seen also in the charge distribution of Ref. [33]. It has the form

$$\rho_{ch}(r) = \rho_0 \frac{1 + \frac{wr^2}{R^2}}{1 + \exp\left(\frac{r-R}{a}\right)} \,. \qquad \text{(A.1)}$$

The three parameters in this form for the charge distribution are, R, a Woods-Saxon radius, a, the diffusivity of that function, and w, a modifying form scale value. Here ρ_0 is the central charge density value with which the volume integral of this distribution leads to the charge of the nucleus (12 for ^{22}Mg).

Normally, the parameters can be constrained to a surface in the 3-dimensional space by requiring the experimentally-known $R^{(c)}_{rms}$. However, there is no experimentally determined $R^{(c)}_{rms}$ value available for ^{22}Mg. Panels (a), (c), and (e) of Fig. A1 each show three 3pF functions with $R^{(c)}_{rms} = 2.888$ fm, $R^{(c)}_{rms} = 3.088$ fm (the value of Ref. [33]), and $R^{(c)}_{rms} = 3.288$ fm. We show the functions in arbitrary units, with $\rho_0 = 1$ e·fm^{-3}. Panels (b), (d) and (f) show the Coulomb potentials that result from the scaled functions, as well as the Coulomb potential assuming a point-like

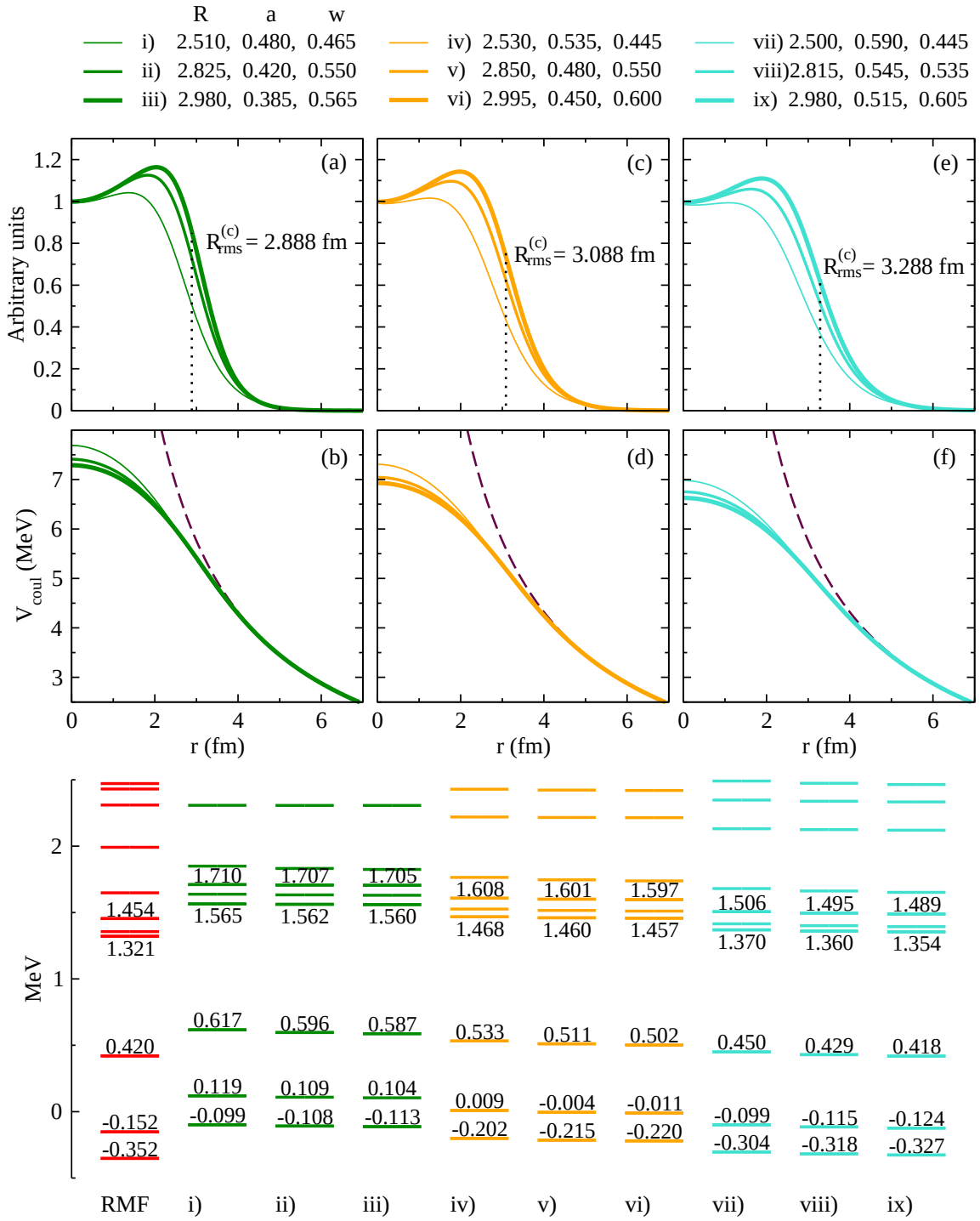

Figure A1. (a) Three 3pF functions which result in charge distributions with $R^{(c)}_{rms} = 2.888$ fm. (b) Resultant Coulomb potentials (solid lines) and potential assuming point-like target (dashed line). (c) Three 3pF functions which result in charge distributions with $R^{(c)}_{rms} = 3.088$ fm. (d) Resultant Coulomb potentials (solid lines) and potential assuming point-like target (dashed line). (e) Three 3pF functions which result in charge distributions with $R^{(c)}_{rms} = 3.288$ fm. (f) Resultant Coulomb potentials (solid lines) and potential assuming point-like target (dashed line). Bottom: Resulting MCAS spectra compared to that resulting from using the RMF charge distribution of Ref. [33].

target. The bottom panel of Fig. A1 shows the MCAS ^{23}Al spectra that result from using these Coulomb potentials with the nuclear potential used in Fig. 2 and 4. The spectrum of Fig. 4, obtained by using the RMF charge distribution of Ref. [33], is also shown.

The different 3pF charge distributions for each value of $R^{(c)}_{rms}$ result in similar spectra of ^{23}Al. As was observed in Ref. [22], parameter variations essentially lead only to an energy shift of the spectrum of a few tens of keV. Changes in $R^{(c)}_{rms}$ result in greater changes in the spectra, of the order of hundreds of keV for the values examined. This reaffirms that when using a 3pF charge distribution, the $R^{(c)}_{rms}$ is the important consideration. The exact values of the parameters (R, a, w) that coincide with the required $R^{(c)}_{rms}$ are of secondary importance.

Comparing the Coulomb potential in panel (b) of Fig. 3 with those of panels (b), (d) and (e) of Fig. A1, we see that the RMF-derived potential differs from those of a 3pF charge distribution in two ways: it has a higher strength at $r = 0$ fm than a potential from a 3pF distribution of lower $R^{(c)}_{rms}$, but has lower strength at larger r, more like a potential derived from a 3pF charge distribution of higher $R^{(c)}_{rms}$.

With these differences in potential we expect variations in calculated observables, and indeed the RMF charge distribution results in lower energies of states than the 3pF distributions with the same $R^{(c)}_{rms}$, by ∼150 keV. This of course means that using a 3pF distribution with this charge radius in Section 4.2 would require less correction to the central well, V_0, of the nuclear potential to find matches to experimentally-known ^{23}Al eigenenergies. However, rather than use the $R^{(c)}_{rms}$ value of Ref. [33] but not that charge distribution, we have opted to use both in absence of experimental guidance.

Appendix B. Observables of the p+^{22}Mg system, $E_{com} = 2.6$ MeV to 3.1 MeV

In Section 4, the parameters of the scattering potential were selected to give the best possible fit to spectral data for the first ∼2 MeV above the ^{23}Al ground state, while predicting the existence of eigenstates up to ∼3.5 MeV, if not their exact energies. Elastic cross sections were predicted for this region of best fit, where no data currently exists.

Elastic scattering differential cross section data, however, do exist for the energy window $E_{com} = 2.6$ to 3.1 MeV, from Ref. [4]. In that study, recoiling protons from the reaction ^{1}H(^{22}Mg,p)^{22}Mg were detected at $\sim 4°$, $\sim 17°$, and $\sim 23°$, which correspond in the centre of mass frame to 172°, 142°, and 134°. It is for the first two of these, and in the centre of mass frame, that elastic scattering cross sections were provided.

We stress that the potential used here is not best suited to this energy window, where the density of states is higher and behaviour other than that of a valence proton above a rotor-like core may affect the spectrum. Additionally, there are almost certainly negative-parity states in this region, but as none have been experimentally observed, we cannot assess their placement by MCAS. However, we have adjusted the V_0^+ well depth to match the MCAS $\frac{3}{2}^+_2$ state's energy with that observed in Ref. [4] at 2.877 MeV relative to the one-proton emission threshold. Additionally, the negative-parity potential was turned off to remove uncertainly from potentially poorly-placed states. The resultant spectrum is shown in Fig. B1, and the resultant cross sections are shown in Fig. B2.

Given the conditions outlined above, the results are reasonable. The resonance feature at ∼2.85 MeV in the data is of different shape than that in the MCAS cross section, but the order of magnitude of the cross section is the same, and the theoretical cross section passes through or near several of the higher-energy data points.

[1] Cerny J, Mendelson Jr R A, Wozniak G J, Esterl J E and Hardy J C 1969 *Phys Rev. Lett.* **22** 612

[2] Wiescher M, Görres J, Sherrill B, Mohar M, Winfield J S and Brown B A 1988 *Nucl. Phys.* **A 484** 90 – 97 ISSN 0375-9474

[3] Caggiano J A, Bazin D, Benenson W, Davids B, Ibbotson R, Scheit H, Sherrill B M, Steiner M, Yurkon J, Zeller A F, Blank B, Chartier M, Greene J, Nolen J A, Wuosmaa A H, Bhattacharya M, Garcia A and Wiescher M 2001 *Phys. Rev.* **C 64**(2) 025802

[4] He J J, Kubono S, Teranishi T, Notani M, Baba H, Nishimura S, Moon J Y, Nishimura M, Iwasaki H, Yanagisawa Y, Hokoiwa N, Kibe M, Lee J H, Kato S, Gono Y and Lee C S 2007 *Phys. Rev.* **C 76**(5) 055802

[5] Gade A, Adrich P, Bazin D, Bowen M D, Brown B A, Campbell C M, Cook J M, Glasmacher T, Hosier K, McDaniel S, McGlinchery D, Obertelli A, Riley L A, Siwek K, Tostevin J A and Weisshaar D 2008 *Phys. Lett.* **B 666** 218

[6] Al-Abdullah T, Carstoiu F, Chen X, Clark H L, Fu C, Gagliardi C A, Lui Y W, Mukhamedzhanov A, Tabacaru G, Tokimoto Y, Trache L and Tribble R E 2010 *Phys. Rev.* **C 81**(3) 035802

[7] Saastamoinen A, Trache L, Banu A, Bentley M A, Davinson T, Hardy J C, Iacob V E, McCleskey M, Roeder B T, Simmons E, Tabacaru G, Tribble R E, Woods P J and Äystö J 2011 *Phys. Rev.* **C 83**(4) 045808

[8] Kirsebom O, Fynbo H, Jokinen A, Madurga M, Riisager K, Saastamoinen A, Tengblad O and Äystö J 2011 *Eur. Phys. J.* **A 47** 130

[9] Banu A, Trache L, Carstoiu F, Achouri N L, Bonaccorso A, Catford W N, Chartier M, Dimmock M, Fernández-Domínguez B, Freer M, Gaudefroy L, Horoi M, Labiche M, Laurent B, Lemmon R C, Negoita F, Orr N A, Paschalis S, Patterson N, Paul E S, Petri M, Pietras B, Roeder B T, Rotaru F, Roussel-Chomaz P, Simmons E, Thomas J S and Tribble R E 2011 *Phys. Rev.* **C 84**(1) 015803

[10] Banu A, Carstoiu F, Achouri N L, Catford W N, Chartier M, Fernández-Domínguez B, Horoi M, Laurent B, Orr N A, Paschalis S, Patterson N, Pietras B, Roeder B T,

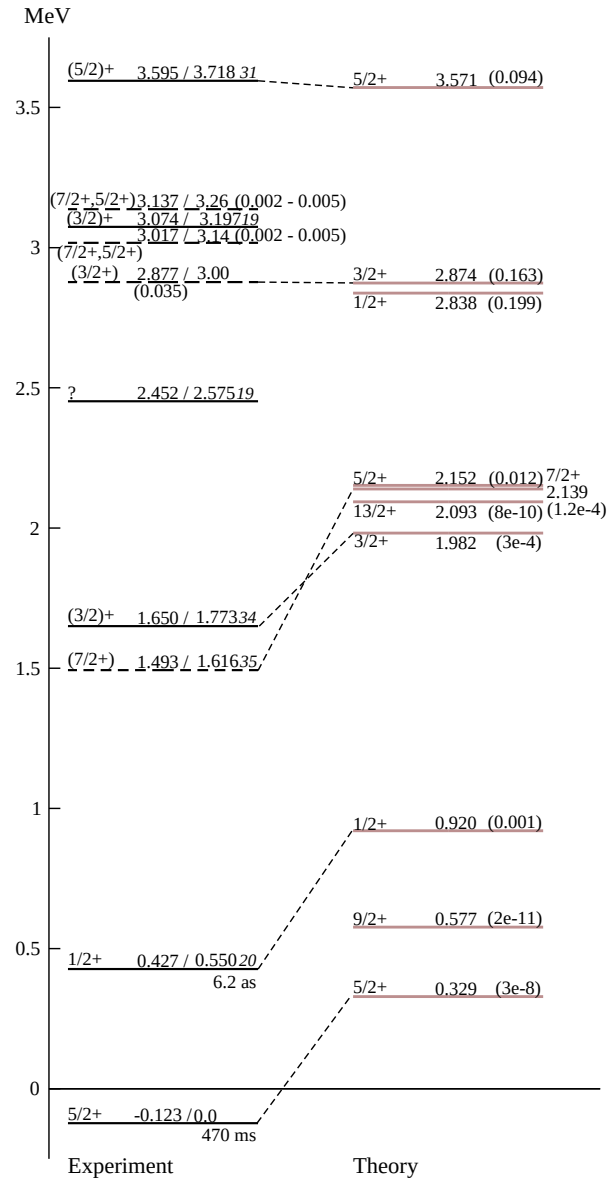

Figure B1. (Color online.) The known experimental ^{23}Al spectrum [4, 5, 26] and that calculated from MCAS evaluation of the p+^{22}Mg, relative to the one proton emission threshold. The MCAS results are obtained with target state set 0^+_1, 2^+_1, 4^+_1, and $\overline{(4)^+_2}$, with charge distribution from Ref. [33]. Positive-parity are as per Table 1, with $V_0^+ = -49.650$ MeV. No negative-parity potential is used. The bar denotes the use of reduced coupling for channels involving this state. In the experimental spectrum, energies before the slash are relative to the one-proton emission threshold, and energies after are relative to the ground state. Uncertainties are shown in italics. In the 'Theory' spectrum, unbracketed values are energy levels relative to one-proton emission threshold. Bracketed values are full widths at half maximum. All energies are in MeV.

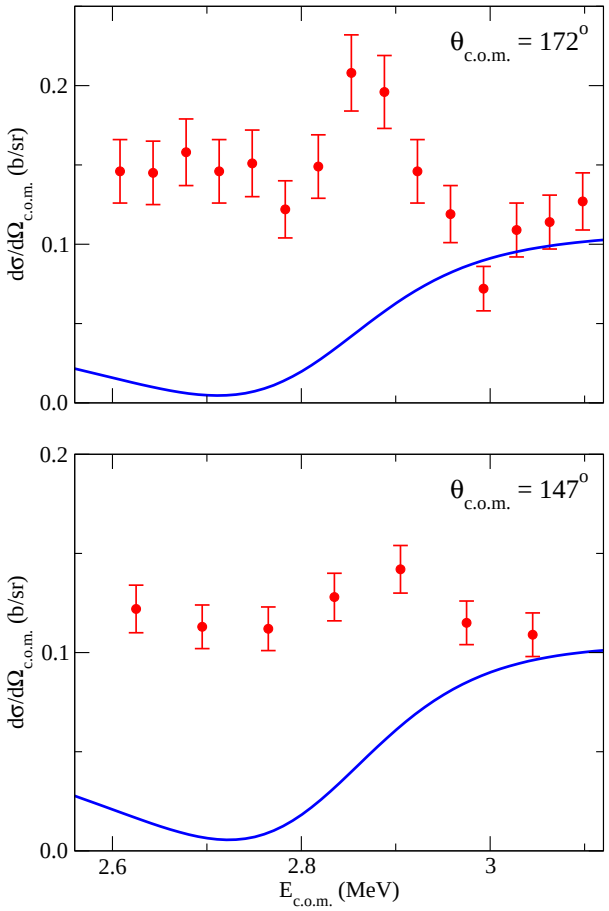

Figure B2. (Color online.) p+^{22}Mg elastic scattering cross section for proton energies from 2.6 to 3.6 MeV at fixed angle (a) 172° and (b) 147° for proton energies from 2.6 to 3.1 MeV. Parameters are as per Table 1, with $V_0^+ = -49.65$ MeV. The experimental data are from Ref. [4].

Roussel-Chomaz P, Thomas J S, Trache L and Tribble R E 2012 *Phys. Rev.* **C 86**(1) 015806
[11] Sherr R 1977 *Phys. Rev.* **C 16**(3) 1159
[12] OXBASH-MSU (the Oxford-Buenos-Aries-Michigan State University shell model code). A. Etchegoyen, W.D.M. Rae, and N.S. Godwin (MSU version by B.A. Brown, 1986); B.A. Brown, A. Etchegoyen, and W.D.M. Rae, MSUCL Report Number 524 (1986)
[13] Yuan C, Qi C, Xu F, Suzuki T and Otsuka T 2014 *Phys. Rev.* **C 89** 044327
[14] Timofeyuk N K and Descouvemont P 2005 *Phys. Rev.* **C 72** 064324
[15] Titus L J, Capel P and Nunes F M 2011 *Phys. Rev.* **C 84** 035805
[16] Amos K, Canton L, Pisent G, Svenne J P and van der Knijff D 2003 *Nucl. Phys.* **A 728** 65
[17] Tamura T 1965 *Rev. Mod. Phys.* **37** 679
[18] Fraser P R, Canton L, Amos K, Karataglidis S, Svenne J P and van der Knijff D 2014 *Phys. Rev.* **C 90** 024616
[19] Saito S 1969 *Prog. Theor. Phys.* **41** 705
[20] Canton L, Pisent G, Svenne J P, Amos K and Karataglidis S 2006 *Phys. Rev. Lett.* **96** 072502
[21] Amos K, Canton L, Fraser P, Karataglidis S, Svenne J and van der Knijff D 2013 *Nucl. Phys.* **A 912** 7
[22] Fraser P R, Amos K, Canton L, Karataglidis S, van der

Knijff D and Svenne J P 2015 *EPJ* **A 51** 110
[23] Basunia M S 2015 *Nucl. Data Sheets* **127** 69
[24] Firestone R B *et al.* 2005 *Nucl. Data Sheets* **106** 1
[25] Davidson J P 1968 *Collective Models of the Nucleus* (New York, London: Academic Press)
[26] Firestone R B *et al.* 2007 *Nucl. Data Sheets* **108** 1
[27] de Vries H, de Jager C W and de Vries C 1987 *At. Data. Nucl. Data* **36** 495
[28] Svenne J P *et al. forthcoming*
[29] Suda T, Wakasugi M, Emoto T, Ishii K, Ito S, Kurita K, Kuwajima A, Noda A, Shirai T, Tamae T, Tongu H, Wang S and Yano Y 2009 *Phys. Rev. Lett.* **102**(10) 102501
[30] Suda T 2014 *Pramana J. Phys.* **83** 739
[31] Serot B D and Walecka J D 1986 *Adv. Nucl. Phys.* **16** 1
[32] Wang Z and Ren Z 2004 *Phys. Rev.* **C 70** 034303
[33] Wang Z and Ren Z 2007 *Nucl. Phys.* **A 794** 47
[34] Chu Y, Ren Z, Wang Z and Dong T 2010 *Phys. Rev.* **C 82**(2) 024320
[35] Timofeyuk N K and Descouvemont P 2005 *Phys. Rev.* **C 71** 064305
[36] Nunes F M, Thompson I J and Johnson R C 1996 *Nucl. Phys.* **A 596** 171
[37] Svenne J P, Amos K, Karataglidis S, van der Knijff D, Canton L and Pisent G 2006 *Phys. Rev.* **C 73** 027601
[38] Canton L and Levchuk L G 2008 *Nucl. Phys.* **A 808** 192
[39] Hodgson P E 1971 *Nuclear Reactions and Nuclear Structure* (Oxford University Press)